Ocean and Coastal Research

BRIEF COMMUNICATION

http://doi.org/10.1590/2675-2824070.22050fd
ISSN 2675-2824

The January 15th, 2022 Hunga Tonga-Hunga Ha'apai eruption recorded in Brazil

Francisco Dourado[1,*], Alessandro Filippo[2], Rogério Candella[3], Lúcio Silva de Souza[2], Domingos Urbano[4], Heitor Evangelista[5], Pedro Costa[6,7]

[1] Universidade do Estado do Rio de Janeiro - Centro de Pesquisa e Estudos sobre Desastres (Rua São Francisco Xavier, 524 - Sala 4038F - Rio de Janeiro - 20550-013 - RJ- Brazil)
[2] Universidade do Estado do Rio de Janeiro - Faculdade de Oceanografia (Rua São Francisco Xavier, 524, Sala 4017E, Rio de Janeiro - 20550-900 - RJ - Brazil)
[3] Instituto de Estudos do Mar Almirante Paulo Moreira (Rua Kioto, 253 - Arraial do Cabo - 28930-000 - RJ - Brazil)
[4] Centro Nacional de Monitoração e Alerta de Desastres Naturais (Estrada Doutor Altino Bondensan, 500 - Distrito de Eugênio de Melo - São José dos Campos - 12247-016 -SP - Brazil)
[5] Universidade do Estado do Rio de Janeiro - Laboratório de Radioecologia e Mudanças Globais (Rua São Francisco Xavier, 524 - Pavilhão Haroldo Lisboa da Cunha - Subsolo - Rio de Janeiro - 20550-013 - RJ - Brazil)
[6] Universidade de Coimbra - Departamento de Ciências da Terra (Rua Sílvio Lima - Pólo II - Coimbra - 3030-790 -Portugal)
[7] Universidade de Lisboa - Faculdade de Ciências - Instituto Dom Luiz (Edifício C1 - Lisboa - 1749-016 - Portugal)

* Corresponding author: fdourado@cepedes.uerj.br

ABSTRACT

Extreme events affect societies all around the world. A recent example is the submarine volcano Hunga Tonga-Hunga Ha'apai in the South Pacific Ocean, which erupted on January 15, 2022 at approximately 0415 UTC, expelling ash up to 39 kilometers high. Instruments around the world recorded both the initial atmospheric shock wave and the subsequent tsunami signal. The aim of this work is to report the record from tide gauges and barometers of this event along the Brazilian coast. For this, the tsunami travel time to Brazil was calculated, and spikes in atmospheric pressure data and noise in the tide gauge records were identified. The arrival of the tsunami waves was clearly observed in tidal records from three stations located in Imbituba, Arraial do Cabo, and Salvador. In addition, in Belém and Santana, the signal-to-noise ratio was too low or there was no signal at all. Surprisingly, the atmospheric signal was less observable. The shock wave signature was evident in the Fortaleza atmospheric pressure data, while at the Imbituba and Belém stations the signal only appeared after filtering the data by calculating the highest and lowest pressure difference within the hour. The weaker, or absence of, barometric signal is likely associated with the supposed attenuation, or blocking, of the signal by the Andes Mountains.

Descriptors: Tsunami, Shock wave, TTT, Tide gauge, Barometer.

The effects of volcanic eruptions can be locally limited or may impact a wide spatial range that can affect global climate conditions (e.g. 2010 Eyjafjallajökull, 1883 Krakatoa). They can also disturb the wave regime, causing loss and damage to coastal areas (e.g. Annak Krakatoa eruption) (International Tsunami Information Center, n.d.).

On January 15, 2022, just before 0415 UTC (Universal Time Coordinated) the submarine volcano Hunga Tonga-Hunga Ha'apai ("Tonga") erupted, ejecting ash over 39 kilometers into the atmosphere. The Tonga submarine volcano is situated in the South Pacific Ocean, 60 km NNW of Nuku'alofa, Tonga at coordinates 20.55°S and

Submitted: 13-May-2022
Approved: 13-Out-2022

Associate Editor: Eduardo Siegle

175.39°W (International Tsunami Information Center, n.d.) (Figure 1). The shock wave and tsunami generated by this event were recorded around the world by various onshore and offshore sensors (e.g. seismometers, tide gauges, and barometers) in addition to satellites in orbit (Amores et al., 2022; Witze, 2022). The volcano is 1800 meters high and 20 kilometers wide and erupts periodically at ca. 20-50 years (Bryan et al., 1972). Together with other submarine volcanoes and more than 130 islands, the Tonga Trench is a submarine ridge along the eastern edge of the Indo-Australian Plate under which the Pacific Plate subducts, forming the second deepest ocean trench in the world at a depth of 10,800 meters. The maximum relative plate motion has been measured at 240 mm/yr (Smith and Price, 2006).

Brazil is situated in a relatively calm area in terms of volcanism, earthquakes, and tsunami activity. However, the atmospheric effects from distant volcanic eruptions have already been recorded on Brazilian territory (de Lima et al., 2012; Lopes et al., 2019). The Brazilian coast is bordered exclusively by the Atlantic Ocean. Despite the long distances traveled, tsunami effects were recorded along the Brazilian coast, such as in the case of the tsunamis in Indonesia of 2004 (distance of approximately 16,000 km) and Japan in 2010 (distance of approximately 17,000 km) (França and De Mesquita, 2007; Candella et al., 2008; Truccolo et al., 2012).

The goal of this brief communication is to present the record of the Tonga volcano explosive eruption event through signals recorded by tide gauges and barometers along the Brazilian coast. This study has three parts: 1. Computation of tsunami travel time (TTT) through analytical computation of the Tonga event; 2. Analysis of atmospheric pressure time series variations detected by barometers at or near sea level monitoring stations along the Brazilian coast; 3. Analysis of sea level time series from tide gauges monitoring stations at specific locations along the Brazilian coast.

Located in South America, Brazil has one of the longest coastlines in the world at 7,491 km. For this work, data used was collected from stations located at Imbituba (SC), Arraial do Cabo (RJ), Salvador (BA), Fortaleza (CE), Belém (PA), and Santana (AP), all port towns of great significance to the Brazilian economy (Figure 1 and Table 1).

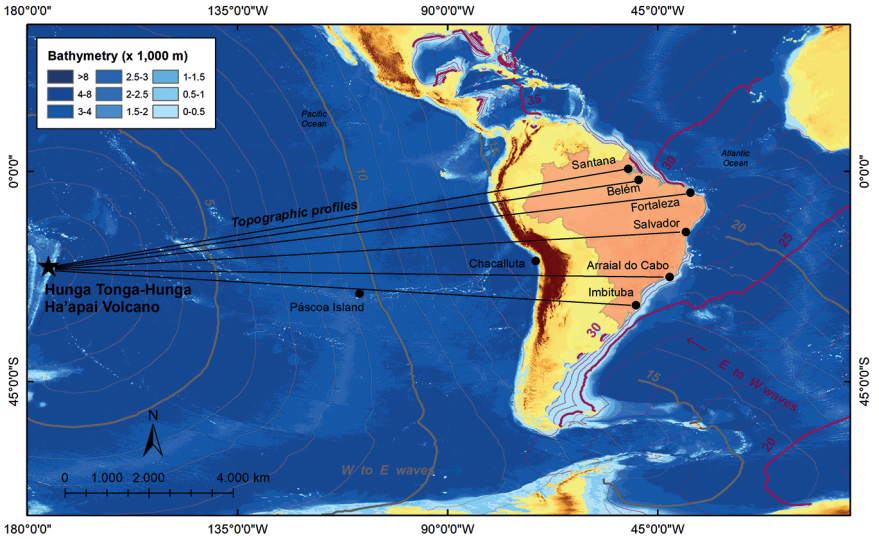

Figure 1. Location map of the Hunga Tonga-Hunga Ha'apai submarine volcano, study area (in light red), monitoring stations, and TTT simulation contour lines (in hours). Bathymetric map with Tonga Volcano (black star) and South America locations. Brazil is filled out and superimposed by the six monitoring station locations (black circles). Additional Chilean stations of Pascoa Island and Chacalula (black circles) were also added. West to east TTT are thin yellow ocean contours, while east to west TTT are thick red contours. Contours numbers are hours.

Table 1. Monitoring stations. Time detection in hours. The arriving time UTC in 16/01/2022. Maximum amplitude in cm.

Station	Coordinates Lat/Long °S/°W	Distance directly from Tonga in km (contouring by ocean)	Tsunami Travel Time Simulations in hours (Arriving time)		Shock wave time detection (Arriving time)	Tsunami time detection (Arriving time) - Max amplitude
			Simulation 1	Simulation 2		
Imbituba (Brazil)	27.817°S 48.57°W	12,000 *(13,200)*	25.27 *(05:31)*	26.47 *(06:43)*	8-9 hours *(16:00-17:00)*	19.04 *(23:17)* -31.0-
Arraial do Cabo (Brazil)	22.956°S 42.0°W	13,000 *(13,800)*	20.01 *(00:16)*	26.48 *(06:44)*	ND 19.20## *(23:38)* -41.5-	17.05 # (21:29) -20.5- 19.20## *(23:38)* -41.5-
Salvador (Brazil)	23:50°W	14,000 *(15,000)*	29.35 *(09:36)*	27.42 (*07:40)*	ND	18.96 *(23:13)* -2.9-
Fortaleza (Brazil)	03.715°S 38.47°W	14,600 *(16,600)*	NC	29.47 *(09:43)*	9-10 hours *(17:00-18:00)*	19.51 *(23:50)* -18.4-
Belém (Brazil)	01.442°S 48.50°W	13,700 *(17,500)*	NC	39.45 *(19:42)*	13-14 hours *(21:00-22:00)*	33.25 *(13:30)* -8.2-
Santana (Brazil)	00.06°S 51.18°W	13,550 *(17,900)*	NC	47.14 *(03:23**)*	NA	ND
Pascua Island (Chile)	27.16°S 109.43°W	6,750 *(6,750)*	9.31 *(13:34*)*	30.08 *(10:20)*	06.22 *(10:28)*	NC
Chacalluta (Chile)	18.36°S 70.34°W	10,700 *(10,700)*	15.18 *(19:26*)*	38.46 *(18:43)*	9.88 *(14:08)*	NC

ND - Not detected; NA - No data available; NC - Not calculated;

* on 15/01/2022; ** on 17/01/2022; # 1st wave; ## 2nd wave

TTT is the time required for the first tsunami wave to propagate from the source to a specific location. Mirone, an open source code written in MATLAB to manipulate large geographic gridded data, was used (Luis, 2007). The code also provides geophysical processing tools, among them one that calculates TTT based on Equation 1:

$$d = t\sqrt{g \times h}$$

where d is the distance traveled by the first wave, t is the time from the beginning of wave propagation, g is the Earth's gravity, and h is the depth of the water column. For this calculation, the bathymetry (water column depth in meters) was obtained from ETOPO1 (Global Relief Model/ NOAA - https://www.ngdc.noaa.gov/mgg/global/).

Considering the global energy propagation of this event, two TTT simulations were performed, Simulation 1 (from west to east) and Simulation 2 (from east to west), each using the Tonga volcano as the tsunami generation mechanism.

The arrival of the atmospheric shock wave from the Tonga volcano explosion was recorded from monitoring stations in Brazil. The atmospheric pressure data used was retrieved from barometers installed at or near the tide gauges stations (Figure 1) and was provided by the National Institute of Meteorology (INMET, https://portal.inmet.gov.br/dadoshistoricos). The higher resolution is an hourly maximum value in millibars (mbar). The gauge network is the Permanent Tidal Network for Geodesy/Brazilian Institute of Geography and Statistics (to be discussed in the next section).

Due to the lack of atmospheric pressure data from the Arraial do Cabo station during the analyzed period, data at the Saquarema station (45 km west), the nearest available station, was used. Similarly, the Imbituba station data was substituted by the Florianopolis station data (70 km north). Given the lack of barometers in near Santana and due to the poor proximity of nearest station (Belém station, ~ 300 km), data from this location was discarded from the analysis.

To achieve a longitudinal distribution of monitoring stations, two Chilean stations were used: Isla de Pascua and Chacalluta (Figure 1). The high-resolution (one-minute) data was obtained from the Dirección Meteorológica de Chile (Dirección General De Aeronáutica Civil - https://climatologia.meteochile.gob.cl/). To standardize the Brazilian and the Chilean atmospheric pressure data, the high-resolution time-series were interpolated into a one-hour time resolution considering the maximum barometric pressure measured in the prior hour.

High-resolution sea level data (1-minute resolution and 1-centimeter vertical precision) from tide gauge monitoring stations were used to check for tsunami wave signals. The astronomical tide series were estimated using the least-squares method of harmonic analysis and then subtracted from the original series. Then, low-frequency oscillations from all residual series were suppressed by the Kaiser-Bessel high pass filter, with a cut-off period of three hours (Candella, 2014).

For the analysis, all six tide gauge stations of the Permanent Tidal Network for Geodesy (RMPG - Rede Maregráfica Permanente para Geodésia) were used: Imbituba, Arraial do Cabo, Salvador, Fortaleza, Belém, and Santana (Figure 1, https://www.ibge.gov.br/geociencias/informacoes-sobre- posicionamento-geodesico/rede-geodesica/10842-rmpg-rede-maregrafica-permanente-para-geodesia.html?=&t=dados-diarios-e-situacao-operacional). The RMPG is a monitoring program for sea level and datum in the Brazilian Institute of Geography and Statistics (IBGE).

The criteria used to determine the arrival of the first wave was the sharp amplification of high-frequency waves with a well-defined dominant period. For this, the signal-to-noise ratio must be favorable, especially when the waves are small. Rabinovich et al., (2011) describe the background noise interference in tsunami wave detection in detail.

Candella, (2014) used energy decay in a uniformly exponential manner formula:

$$E(t) = E_0.e - ^{\delta t}$$

where E_0 is the tsunami energy index, δ is the energy decay (attenuation) coefficient, and t_0 = δ−1 is the "decay time." In order to compute the variance evolution, a six hour segment with three hour overlap was used, resulting in one variance value every three hours. The decay line was set by the least square method.

The residual data series were weighted for application of the wavelet transform developed by Grossmann and Morlet (1984), an alternative to the Fourier transform. The wavelet transform has an advantage over classical spectral analyses because it allows for the analysis of the periodicity of events at different scales of temporal variability (frequencies and time scales) and does not require a stationary series (Santos et al., 2013).

In this work, two propagation analytical simulations of the first tsunami wave were produced for the Tonga event. A time-series analysis of barometric, sea level, atmospheric pressure, and tide gauge data were collected at monitoring stations along the coast of Brazil. The simulations were compared to the tide gauge data, while the atmospheric pressure data was used to demonstrate the shock wave arrival in South America.

According to the first tsunami wave propagation simulations, the Brazilian coast was reached two times by waves generated by the eruption of the Tonga volcano. First, from west to east (Simulation 1), and subsequently from east to west (Simulation 2).

Simulation 1 shows the waves traversing the narrow Drake Passage (650-km wide) from west to east; the TTT to the southernmost area of the Brazilian coast was 27.27 hours. Due to a shadow zone on the northern Brazilian coast near the Caribbean, the comparison and validation of the modeled TTT based on the monitoring stations is

somewhat limited. Therefore, it was not possible to compare the simulation with the Fortaleza, Belém, and Santana stations (Figure 1 for locations).

Simulation 2 shows the waves flowing from the Pacific Ocean, running through the Indian Ocean, entering the Atlantic Ocean along the Cape of Good Hope, and later reaching the Brazilian coast. From this direction, the computed TTT was 27.00 hours and 32.67 hours to the southernmost and northernmost areas of the Brazilian coast, respectively (Table 1).

Using available databases, shock wave signal detection was not obvious in several atmospheric pressure datasets (1-h resolution) from the monitoring stations on the Brazilian coast, with the exception of the Fortaleza station (Figure 2, green continuous lines).

After calculating the difference between the maximum atmospheric pressure and the minimum atmospheric pressure of the previous hour to highlight the attenuated signal, the result displays two new pressure peaks from the Imbituba and Belém stations (Figure 2, dashed blue and dark blue lines, respectively), as well as from the Fortaleza station (already evidenced in the hourly maximum atmospheric pressure graph).

The arrival of the tsunami signal at each station is clear when one observes the filtered residuals series from each station (Figure 2). In the case of Arraial do Cabo and Salvador stations, two periods with energy peaks were detected. Arraial do Cabo showed an energy peak at approximately 16 min and 128 min, while the Salvador station showed energy peaks at approximately 32 min and 128 min. All other stations exhibited only one energy peak, in the vicinity of 128 minutes. The distance from the eruption site and the differences in the continental shelf width along the Brazilian coast interfered with the arrival times. For instance, one could expect the tsunami wave would reach Imbituba before Arraial do Cabo. However, the continental shelf near Imbituba (~124 km) is wider than near Arraial do Cabo (~75 km), leading to a reduction in tsunami wave celerity and thus delaying the arrival at Imbituba.

The northernmost stations (Fortaleza, Belém, and Santana) were influenced by other local meteorological factors that were intense despite signal filtering; the tsunami signal was either smoothened or absent. At the Belém station, the signal displayed high oscillations every day between 3pm and 9pm, possibly associated with sea-breeze forcing between December and May (Bastos et al., 2002).

The TTT calculated for each monitoring station is consistent with the expected arrival time considering the increasing distance from the source; the farther the station, the longer the TTT (Table 1). In the South Atlantic, TTT measured values can diverge from TTT simulated values due to tidal variation or, occasionally, because they may have been disturbed by the superposition of the west to east direction over east to west waves (Figure 1), as observed for the 2004 Sumatra tsunami by Rabinovich et al. (2011). Both events were of magnitudes that allowed for wave propagation through several oceans. With similar propagation speeds in both directions (east to west and west to east), the waves met on the opposite side of the planet. In this region, the waves interact with each other, adding or decreasing amplitude and speed.

The TTT simulations for the Imbituba (extreme south of the study area), Belém, and Santana (extreme north of the study area) monitoring stations yield higher than the expected times of arrival due to the extensive shallow offshore profile (continental shelf) of these regions on the Brazilian coast. This delay can also be explained based on the wave propagation equation (1) used in the TTT modeling, which better describes wave speeds in deeper areas (Rabinovich et al., 2011; Watada et al., 2014; An and Liu, 2016).

The time of arrival of the shock wave was not observed in barometric pressure data, raising doubt as to whether the arrival signal was not actually recorded at these stations or if the signal had been eliminated or attenuated due to the hourly temporal resolution of the data.

To test the first hypothesis, an experiment was designed to verify if the shock wave could be observed in data of hourly resolution. Data from the Chilean stations Isla de Pascua and Chacalluta (situated along the path of the Tonga tsunami, between the source and the Brazilian stations) were thus resampled for hourly resolution. The arrival of the shock wave continued to be observed in this data despite the lower time resolution.

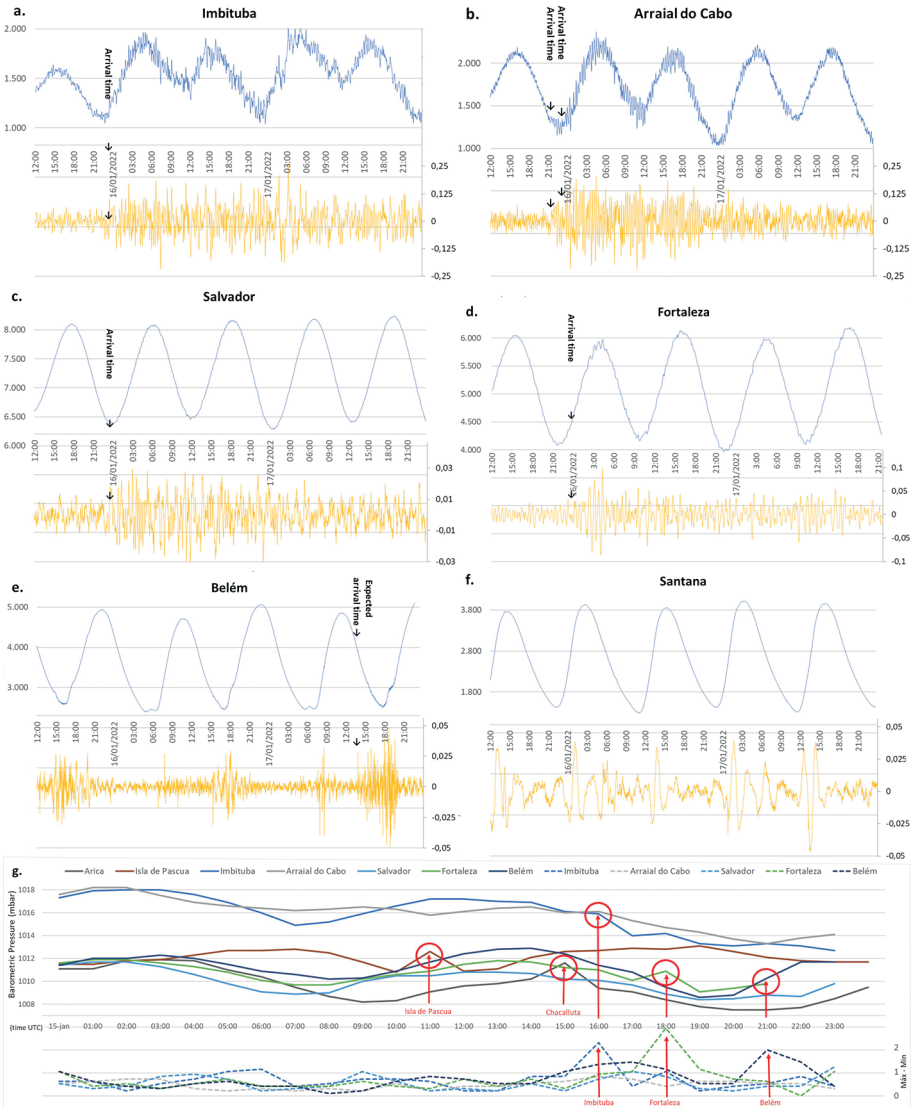

Figure 2. Observed data: tide gauge data (in meters) on monitoring stations (measured signal in blue, residual filtered signal in orange) for Imbituba (a.), Arraial do Cabo (b.), Salvador (c.), Fortaleza (d.), Belém (e.), and Santana (f.). Barometric Pressure time series (g.). Upper profiles are the Maximum Barometric Pressure during prior hours (lines). Dashed lines are the difference between Maximum Barometric Pressure and Minimum Barometric Pressure during prior hours.

To test the second hypothesis, the increase in atmospheric pressure was boosted by calculating the difference between the maximum atmospheric pressure and the minimum atmospheric pressure of the prior hour, instead of observing only the maximum atmospheric pressure of the prior hour. With this filter, we observed two new pressure peaks at the Imbituba and Belém stations (Figure 2).

A possible explanation for the barometric signal attenuation could be that the shock wave signal weakened due to topographic blocking from the Andes, as they are on the topographic profile between the Tonga volcano and the monitoring stations in Brazil.

Signs of the Tonga tsunami wave on tide gauges appear in the series of sea level variations from Imbituba, Arraial do Cabo, Salvador,

and Fortaleza stations. Arrival times are compatible with those simulated by TTT, as shown in Table 1. However, the same cannot be said for the data from the Belém and Santana stations, where the same filtered signal shows other oscillations, of local character, that mask the tsunami signal; it is not certain that the tsunami signal was present.

The river breeze (RB) is a phenomenon associated with precipitation regimes, with different aspects than terrestrial and sea breezes. In the Region of Belém city (near the Equator), the RB is strong and frequently observed year-long between 1200-0000 UTC. Surface behavior of waves is affected by RB. Considering the low amplitude of the tsunami-related wave component, the RB may significantly impact the sea level-change signal identified in Figure 2e (Belém station). Land breeze (LB) signals are more frequent between March and May, but the signal peak around 0700 LT may also be associated with this pattern (Germano et al., 2017). The daily wind cycle associated with LB is more intense at ~1000 UTC (~2200 UTC) on the shore around Belém city. This corresponds to ~0700 LT (~1900 LT), and that higher frequency is generally related to lower interannual variability, with a significant correlation between the interannual variability of the frequency and oceanic indices along specific coastal areas (Souza and Oyama, 2017). These aspects help better understand the signal observed at Belém and Santana, where the peaks (Figure 2) are related to these forces; this makes it difficult to identify the tsunami signal in these locations. At the Belém Station, the signal intensity recorded on 01/17/2022 at approximately 1300 LT may be a signal of the tsunami. The wave spectral analysis of the residual signal at the Arraial do Cabo and Salvador stations showed two energy peaks at different periods, with the prominent peak having a period of 128 minutes due to its energy. These peaks may be related to tsunami formation from distinct sources, the volcano's explosion and the sudden change in atmospheric pressure. Despite local effects, it was possible to perceive the effects of the tsunami waves along the coast of Brazil.

In Brazil, the eruption of the Tonga volcano was recorded in tide gauges and barometers. The TTT simulations for Arraial do Cabo, Salvador, and Fortaleza produced reliable results. For the Imbituba, Belém, and Santana monitoring stations, the travel time was higher than expected due to the extensive shallow offshore profile, thus affecting the wave propagation equation (1) used in the TTT modeling. Finally, the tsunami signal was clearly observed in the tide gauges from the southern region of the study area. At Imbituba and Arraial do Cabo stations, the maximum wave amplitudes reached 31 and 41.5 cm, respectively.

The record of the shock wave propagation was clearly observed at the Fortaleza monitoring station (Figure 2). The absence of any weak signal at the other stations was supposedly due to the natural barrier formed by the Andes mountain range.

There is a false perception that far-sourced tsunamis do not affect very distant coastlines. This work demonstrates that this is not accurate. Areas like Brazil, even if very distant from tsunami sources, need to prepare for the impacts of natural disasters. The low values of maximum wave amplitude (41.5 cm) in low altitude regions and associated syzygy tide events can induce losses and damages. The results of this work highlight the importance and need to map tsunamigenic risk and advance tsunami monitoring programs along the Brazilian coast.

ACKNOWLEDGMENTS

Francisco Dourado acknowledges FAPERJ for the support provided through the "Young Scientist of Our State" fellowship (E-26/202.665/2018). Pedro Costa acknowledges the financial support of FCT through project OnOff – PTDC/CTAGEO/28941/2017. Heitor Evangelista thanks the INCT-Criosfera.

AUTHOR CONTRIBUTIONS

F.D..: Conceptualization; TTT simulation; Writing, review & editing - original draft;

A.F.: Tide gauge data processing and interpretation; Review & editing;

R.C..: Tide gauge data processing and interpretation (*in memoriam*);

L.S.S.: Meteorological interpretation; Review & editing;

D.U.: Tide gauge data processing and interpretation; Review & editing;

H.E.: Barometric data processing and interpretation; Review & editing;

P.C.: TTT data processing and interpretation; Writing, review & editing.

REFERENCES

AMORES, A., MONSERRAT, S., MARCOS, M., ARGÜESO, D., VILLALONGA, J., JORDÀ, G. & GOMIS, D. 2022. Numerical simulation of atmospheric lamb waves generated by the 2022 hunga-tonga volcanic eruption. *Geophysical Research Letters*, 49(6), e2022GL098240, DOI: https://doi.org/10.1029/2022GL098240

AN, C. & LIU, P. L. F. 2016. Analytical solutions for estimating tsunami propagation speeds. *Coastal Engineering*, 117, 44-56, DOI: https://doi.org/10.1016/j.coastaleng.2016.07.006

BASTOS, T. X., PACHECO, N. A., NECHET, D. & SÁ, T. D. A. 2002. *Aspectos climáticos de Belém nos últimos cem anos*. Belém, PA: Embrapa Amazônia Oriental.

BRYAN, W. B., STICE, G. D. & EWART, A. 1972. Geology, petrography, and geochemistry of the volcanic islands of Tonga. *Journal of Geophysical Research*, 77(8), 1566-1585, DOI: https://doi.org/10.1029/JB077i008p01566

CANDELLA, R. N. N. 2014. Statistical and spectral characteristics of the 2011 East Japan tsunami signal in Arraial do Cabo, RJ, Brazil. Revista Brasileira de Geofísica, 32(2), 235, DOI: https://doi.org/10.22564/rbgf.v32i2.480

Candella, R. N., RABINOVICH, A. B. & THOMSON, R. E. 2008. The 2004 Sumatra tsunami as recorded on the Atlantic coast of South America. *Advances in Geosciences*, 14, 117-128, DOI: https://doi.org/10.5194/adgeo-14-117-2008

FRANÇA, C. A. S. & MESQUITA, A. R. 2007. The December 26th 2004 tsunami recorded along the Southeastern Coast of Brazil. *Natural Hazards*, 40(1), 209-222, DOI: https://doi.org/10.1007/s11069-006-0010-1

GERMANO, M. F., VITORINO, M. I., COHEN, J. C. P., COSTA, G. B., SOUTO, J. I. O., REBELO, M. T. C. & SOUSA, A. M. L. 2017. Analysis of the breeze circulations in Eastern Amazon: an observational study. *Atmospheric Science Letters*, 18(2), 67-75, DOI: https://doi.org/10.1002/asl.726

GROSSMANN, A. & MORLET, J. 1984. Decomposition of hardy functions into square integrable wavelets of constant shape. *SIAM Journal on Mathematical Analysis*, 15(4), 723-736, DOI: https://doi.org/10.1137/0515056

ITIC (INTERNATIONAL TSUNAMI INFORMATION CENTER). 2022. *15 January 2022, Hunga-Tonga-Hunga-Ha'apai Volcanic Eruption* [online]. Honolulu: ITIC. Available at: http://itic.ioc-unesco.org/index.php?option=com_content&view=article&id=2186&Itemid=3265. Accessed: 2020 May 01.

LIMA, E. F., SOMMER, C. A., SILVA, I. M. C., NETTO, A. P., LINDENBERG, M. & ALVES, R. C. M. 2012. Morfologia e química de cinzas do vulcão Puyehue depositadas na região metropolitana de Porto Alegre em junho de 2011. *Revista Brasileira de Geociências*, 42(2), 265-280, DOI: https://doi.org/10.5327/Z0375-75362012000200004

LOPES, F., SILVA, J., MARRERO, J., TAHA, G. & LANDULFO, E. 2019. Synergetic aerosol layer observation after the 2015 calbuco volcanic eruption event. *Remote Sensing*, 11(2), 195, DOI: https://doi.org/10.3390/rs11020195

LUIS, J. F. 2007. Mirone: a multi-purpose tool for exploring grid data. *Computers & Geosciences*, 33(1), 31-41, DOI: https://doi.org/10.1016/j.cageo.2006.05.005

RABINOVICH, A. B., WOODWORTH, P. L. & TITOV, V. V. 2011. Deep-sea observations and modeling of the 2004 Sumatra tsunami in Drake Passage. Geophysical Research Letters, 38(16), DOI: https://doi.org/10.1029/2011GL048305

SANTOS, C., FREIRE, P. & TORRENCE, C. 2013. A transformada wavelet e sua aplicação na análise de séries hidrológicas. *RBRH*, 18(3), 271-280, DOI: https://doi.org/10.21168/rbrh.v18n3.p271-280

SMITH, I. E. M. & PRICE, R. C. 2006. The Tonga-Kermadec arc and Havre-Lau back-arc system: Their role in the development of tectonic and magmatic models for the western Pacific. *Journal of Volcanology and Geothermal Research*, 156(3-4), 315-331, DOI: https://doi.org/10.1016/j.jvolgeores.2006.03.006

SOUZA, D. C. & OYAMA, M. D. 2017. Breeze potential along the brazilian northern and northeastern coast. *Journal of Aerospace Technology and Management*, 9(3), 368-378, DOI: https://doi.org/10.5028/jatm.v9i3.787

TRUCCOLO, E. C., SCHETTINI, C. A. F. & ALMEIDA, D. 2012. The 2004 Sumatra tsunami effect on the Itajaí-Açu estuary water level, Santa Catarina, Brazil. *Brazilian Journal of Oceanography*, 60(3), 461-466, DOI: https://doi.org/10.1590/S1679-87592012000300017

WATADA, S., KUSUMOTO, S. & SATAKE, K. 2014. Travel-time delay and initial phase reversal of distant tsunamis coupled with the self-gravitating elastic Earth. *Journal of Geophysical Research: Solid Earth*, 119(5), 4287-4310, DOI: https://doi.org/10.1002/2013JB010841

WITZE, A. 2022. Why the Tongan eruption will go down in the history of volcanology. *Nature*, 602(7897), 376-378, DOI: https://doi.org/10.1038/d41586-022-00394-y